［溶接学会論文集　第 33 巻　第 2 号　p. 20s-24s（2015）］

Theoretical Analysis for Solidification Cracking Susceptibility in Type 316FR Stainless Steel Laser Welds*

by Eun-Joon Chun**, Hayato Baba**, Kazutoshi Nishimoto*** and Kazuyoshi Saida****

For quantitative evaluation of solidification cracking susceptibility in two kinds of type 316FR stainless steel (316FR-A and 316FR-B) laser welds, laser beam welding (LBW) transverse-Varestraint test was performed. As the welding speed increased from 1.67 to 40.0 mm/s, enlargement range of solidification brittle temperature range (BTR) for 316FR-B (from 14 to 40 K) was larger than that for 316FR-A (from 37 to 46 K), respectively. Based on theoretical calculations for solid/liquid coexistence temperature range by using Kurz-Giovanola-Trivedi and solidification segregation models, the reason for larger increment of the BTR for 316FR-B could be regarded as larger decrement of δ-ferrite amount during the welding solidification than that for 316FR-A, affecting severe increment of the impurities' segregation (S and P), thereby more enlarging the solid/liquid coexistence temperature range as compared with that of 316FR-A.

Key Words: Laser Beam Welding, Transverse-Varestraint Test, Solidification Brittle Temperature Range, Solidification Segregation

1. Introduction

Among the diverse types of nuclear power generation, the fast breeder reactor (FBR, using fast neutrons that breed Plutonium-239 from Uranium-238) is well known as the most advanced reactor owing to its superior fuel economy. Type 316FR stainless steel, which has improved creep fatigue property over other austenitic stainless steels, is likely to be used for the structural material of the primary coolant circuit in the next generation of commercial FBR plants [1]. Meanwhile, when the FBR plants have been in operation for a long time, maintenance of their aging components, which mainly involve welding processes, will become essential procedure. For this purpose, laser clad welding has been considered as one of the most effective candidates owing to several merits on laser beam welding (LBW) process for both manufacturing and metallurgical aspects [1]. During LBW of austenitic stainless steels, special attention should be paid to the weldability, which is commonly examined in terms of solidification cracking [2]. In the present study, based on the developed the Varestraint testing setup assembled with LBW apparatus (LBW transverse-Varestraint test) [3], effect of welding speed on solidification brittle temperature range (BTR) in laser welds of type 316FR stainless steels was quantitatively investigated. Also, the variation mechanism of BTR was discussed by theoretical analysis on solid/liquid coexistence temperature range during non-equilibrium solidification process, considering dendrite supercooling, diffusion and the solidification segregation.

*Received: 2014.11.28
**Student Member, Graduate school of Engineering, Osaka University
***Member, Graduate school of Engineering, Fukui University of Technology
***Member, Graduate school of Engineering, Osaka University

2. Materials and experimental procedures

2.1 Materials

The materials used in this study are two types (316FR-A, 316FR-B) of filler metal for type 316FR stainless steel. The chemical composition (mass%) of the 316FR-A is 0.0085 C-0.0009S-0.023P-17.5Cr-12.0Ni-2.1Mo-0.4Si-0.8Mn-0.09N, and the 316FR-B is 0.005C-0.001S-0.029P-18.51Cr-11.50Ni-2.28 Mo-0.47Si-1.5Mn-0.067N for 316FR-B. The Cr_{eq}/Ni_{eq} value indicates 316FR-A has solidification with AF (primary austenite and secondary δ-ferrite) mode and FA (primary δ-ferrite and secondary austenite) mode for 316FR-B [4], respectively.

2.2 Transverse-Varestraint test with laser beam welding

Fig. 1 shows schematic description for the LBW transverse-Varestraint test with dimension and arrangement of specimen for the test (laser oscillator: multi-mode fiber laser, maximum power: 6 kW). Two levels of the welding speed (20.0 and 40.0 mm/s) were employed for the transverse welding, and the laser power was adjusted to obtain a half-penetration bead at each welding speed. The beam radius was 0.4 mm, and defocus distance at the specimen surface was 0 mm for the transverse welding. The length of transverse welding was 30 mm at each welding speed. The augmented strain was varied between 0.25 and 5.88 %. The tested surface after the transverse-Varestraint test was observed by a scanning electron microscope (SEM) to quantify length of cracks. The temperature history (cooling rate) during the solidification of transverse welding was measured using a thermocouple (W-Re, diameter: 0.6 mm) directly plunged into the molten pool during the transverse welding to obtain the cracking temperature range.

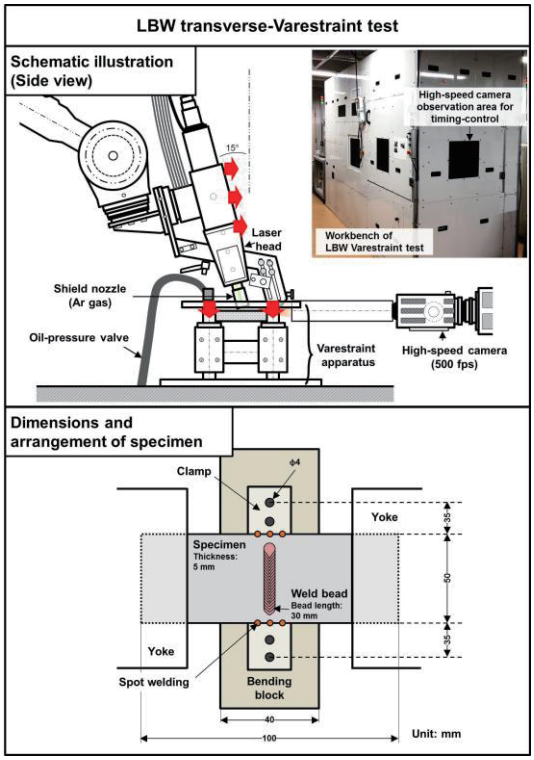

Fig. 1 Schematic descriptions on LBW transverse-Varestraint test and specimen dimensions used.

3. Effect of welding speed on solidification brittle temperature range

Fig. 2 summarizes variation behavior of the BTR for both 316FR-A and 316FR-B as a function of the welding speed from 1.67 mm/s (conventional transverse-Varestraint test with gas tungsten arc welding: GTAW transverse-Varestraint test) to 40.0 mm/s (LBW transverse-Varestraint test). The BTR for the GTAW transverse-Varestraint test was referred to the author's previous study in Ref. 1. The BTR enlarged from 37 to 46 K (for 316FR-A), and from 14 to 40 K (for 316FR-B). It follows that the solidification cracking susceptibility for 316FR-A and 316FR-B steels enhanced through the application of LBW process. Especially, the range of BTR enlargement in 316FR-B (26 K) was larger than that of 316FR-A (9 K). The governing factor of the BTR variation was discussed by theoretical calculations on solid/liquid coexistence temperature range during the welding solidification.

4. Variation mechanism of solidification cracking susceptibility in laser welds

The mechanism of different enlargement behavior for BTR in 316FR-A and 316FR-B with an increase in welding speed was discussed by employing a numerical calculation of the solid/liquid coexistence temperature range in LBW. Generally,

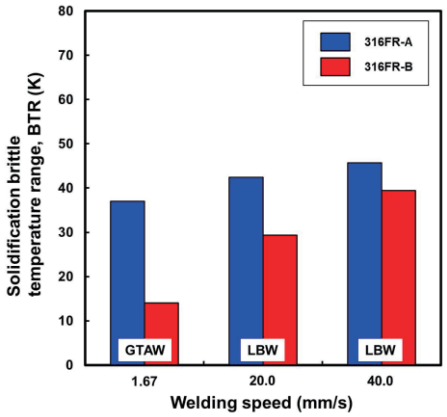

Fig. 2 Relationship between BTR and welding speed for both 316FR-A and 316FR-B.

the BTR is characterized by upper and lower temperature limits. The upper temperature limit of the BTR approximately corresponds to the solidification initiation temperature (T_I), which can be also expressed by the nominal liquidus temperature (T_L). The solidification completion temperature also approximates the lower temperature limit of the BTR. During the welding process, segregation of solute elements occurs along with dendrite growth because a solid phase exhausts solute elements into the remaining liquid phase. Consequently, the solute content of the liquid continuously increases during the solidification. Thus, the true solidification completion temperature (T_C) deviates from the nominal solidus temperature (T_S). A difference between solidification initiation (T_I) and the completion (T_C) temperatures could be regarded as the solid/liquid coexistence temperature range ($T_I - T_C$) during the welding solidification. Therefore, the variation mechanism of the solid/liquid coexistence temperature range ($T_L - T_C$) as a function of the welding speed would govern the BTR change mechanism. The changes in solidification initiation (T_I) and completion (T_C) temperatures were computed using the Kurz-Giovanola-Trivedi (KGT) model [5] and a solidification segregation model, respectively.

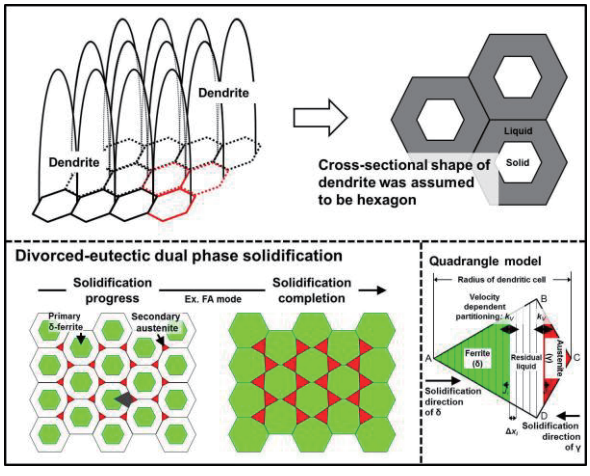

Fig. 3 Schematic descriptions on solidification segregation model.

4.1 Theoretical calculation of solidification initiation and completion temperatures

Firstly, the solidification initiation temperature (T_I) can be approximated by the dendrite tip temperature. In order to calculate the dendrite tip temperature, the KGT model extended for Fe-Cr-Ni ternary system has been applied [2]. The calculation procedure is similar to that used in several studies already reported [2,3], and Eq. 1 shows a brief description as follows;

$$T_I = T_L^{eq} - \sum_i m_i^{eq} C_i^0 \left\{ 1 - \frac{1 + \dfrac{k_i^{eq} - k_i^V \left(1 - \ln \dfrac{k_i^V}{k_i^{eq}}\right)}{1 - k_i^{eq}}}{1 - \left(1 - k_i^V\right) I_V\left(P_i^C\right)} \right\} - \frac{2\Gamma}{R} - \frac{R_g T_m^2}{\Delta H_f V_0} V - \frac{GD}{V} \qquad (1)$$

where T_L^{eq} is equilibrium liquidus temperature, m_i^{eq} is equilibrium liquidus slope, C_i^0 is the initial composition of alloying elements, k_i^{eq} is equilibrium partitioning coefficient, k_i^V is velocity-dependent partitioning coefficient, $I_V\left(P_i^C\right)$ is Ivantsov's solution, Γ is Gibbs-Thompson parameter, R_g is gas constant, T_m liquidus temperature of pure iron, H_f is enthalpy of fusion, V_0 is the sonic velocity in liquid.

Secondly, in order to calculate the solidification completion temperature (T_C), the solidification segregation behaviors of all solute elements to the cell boundary were calculated for each binary system (i.e. Fe-Cr, Ni, Mo, Si, Mn, P, S, C and N) using the finite differential method. Divorced-eutectic solidification model (half-quadrangle model) was adopted. Fig. 3 shows schematic description for this segregation model. The model assumed that cross-sectional shape of a dendrite is a hexagonal prism. The principle of the calculation procedure is similar to those previously reported [2,3,6]. Below is a brief description of this segregation model.

The distribution of the solute elements during the solidification process was determined by solving the diffusion equation for both solid and liquid phases. Symmetrical boundary conditions were applied to the both end segments. The diffusive flux J_i from a segment i to a segment $i+1$ is given by Fick's first law;

$$J_i = D \frac{C_{i+1} - C_i}{\Delta x} \qquad (2)$$

where D is the diffusion coefficient of the solute, C_i and C_{i+1} are the concentrations in segment i and $i+1$ respectively, and Δx is the segment width. The change in solute concentration ΔC_i during a minute time interval Δt at segment i is expressed by;

$$\frac{\Delta C_i}{\Delta t} \frac{S_i + S_{i-1}}{2} \Delta x_i = J_i S_i - J_{i-1} S_{i-1} \qquad (3)$$

where S_i and S_{i-1} are the sectional areas of segments i and $i-1$ respectively. S_i is expressed as Eq. 4;

$$S_i = \frac{1}{2\sqrt{3}} \left(\sum_{k=1}^{i} \Delta x_k \right)^2 \qquad (4)$$

From Eqs (3) and (4), ΔC_i can be found from;

$$\Delta C_i = \frac{2D\Delta t}{\Delta x_i (S_i + S_{i-1})} \left\{ S_i \frac{C_{i+1}^B - C_i^B}{\Delta x_i} - S_{i-1} \frac{C_i^B - C_{i-1}^B}{\Delta x_{i-1}} \right\} \qquad (5)$$

where C_{i+1}^B, C_i^B and C_{i-1}^B are the solute concentrations in segment $i+1$, i and $i-1$ at the previous Δt. Assuming the mass conservation law of solute in a dendrite, Eq. (6) can be obtained.

$$\left(\sum_{k=1}^{N} \Delta x_k \right)^2 C_0 = \sum_{i=1}^{N} \left\{ \left(\sum_{k=1}^{i} \Delta x_k + \sum_{k=1}^{i-1} \Delta x_k \right) \Delta x_i C_i^S \right\} + \sum_{i=j+1}^{N} \left\{ \left(\sum_{k=1}^{i} \Delta x_k + \sum_{k=1}^{i-1} \Delta x_k \right) \Delta x_i C_i^L \right\} \qquad (6)$$

where N is the total number of segments, C_0 is the initial solute concentration, C_i^S is the solute concentration in solid phase segment i, C_i^L is the solute concentration in the liquid phase and j is the segment number of the solid phase at the solid/liquid interface.

During the solidification process, the solute concentration at the solid/liquid interface is determined by the non-equilibrium concept as follows;

$$C_j^S = k_V C_{j+1}^L \qquad (7)$$

where C_j^S, C_{j+1}^L are the solute concentrations of solid and liquid phases at the solid/liquid interface, and k_V is the non-equilibrium distribution coefficient. The solidification segregation was computed by 95% solidification completion (i.e. fraction of residual liquid phase was 5%) [2,3]. The segregated concentration of all solute elements in the residual liquid phase at solidification completion (= 95% solidification completion) was inputted to Thermo-Calc software (SSOL4 database), and the equilibrium solidus temperature computed by the Thermo-Calc was adopted as the solidification completion temperature (T_C) in the welding solidification.

Material constants used in the calculation for both the solidification initiation and completion temperatures were referred by Refs. 2,3,7. The equilibrium liquidus temperatures of the steels used were obtained from the Thermo-Calc software with the SSOL4 database. For simplicity, all the calculations were carried out under the following assumptions; the dendrite solidification velocity is equal to the welding speed, the cooling rate remains constant during solidification, and interactions between solute elements (i.e. cosegregation) are negligible. The

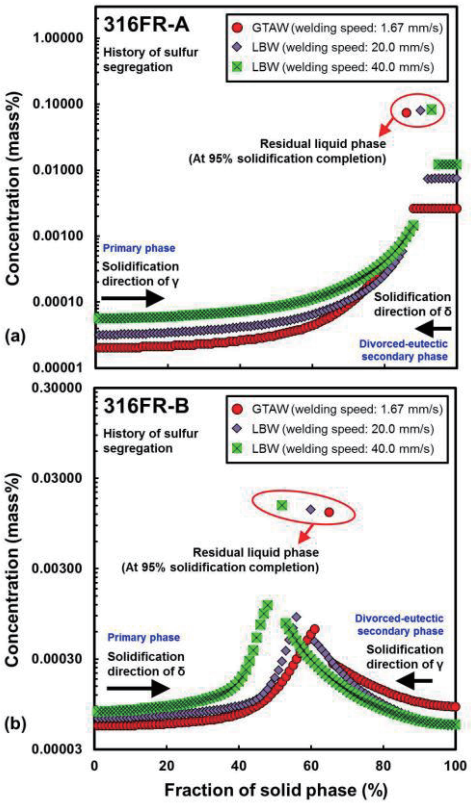

Fig. 4 Calculated solidification segregation behavior for (a) 316FR-A and (b) 316FR-B.

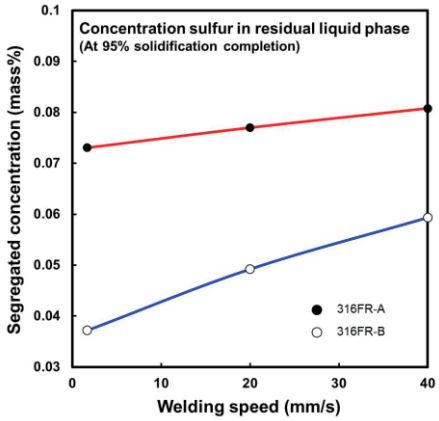

Fig. 5 Relationship between segregated concentration of impurities (S, P) and welding speed.

dendrite radius employed was 10.0 μm, and the mesh was divided into 100 segments. The welding speed was varied as 1.67 mm/s (GTAW) and 20.0, 40.0 mm/s (LBW). For both steels, the cooling rate during solidification was assumed to be 240 K/s for 1.67 mm/s (GTAW), 1200 K/s for 20.0 mm/s (LBW), and 1950 K/s for 40.0 mm/s (LBW) based on the measured thermal cycle during the transverse welding.

4.2 Solidification segregation behavior of impurities

Among various alloying elements in stainless steels, sulfur (S) and phosphorous (P) have been generally regarded as the most governing elements of the solidification cracking susceptibility (especially the solidification cracking temperature range), easily segregating at the remaining liquid phase between dendrites during the welding solidification [2,4]. Fig. 4 representatively shows the calculated segregation behavior of S for both 316FR-A and 316FR-B. During the welding solidification, the S concentration increased with the progress of the solidification, and high amounts of S were segregated to the remaining liquid phase at solidification completion (indicating respective peak concentration between austenite and δ-ferrite for both 316FR-A and 316FR-B) in every welding speed. As the welding speed increased, S was easily distributed in the solid phase. And the fraction of constituent phases (austenite and δ-ferrite) during the solidification was also varied at each welding speed. As a result, segregated concentration of S in the residual liquid phase at the solidification completion was also different in accordance with the welding speed. Fig. 5 shows variation of the segregated concentrations in remaining liquid phase at solidification completion as a function of the welding speed for both S and P. Although the segregated concentrations of S and P increased with an increase in the welding speed for both 316FR-A and 316FR-B welds, increment range of the concentration for 316FR-B was larger than that of 316FR-A. In other words, it could be confirmed that behavior of the impurities' segregation during the solidification as a function of welding speed was also different between 316FR-A and 316FR-B.

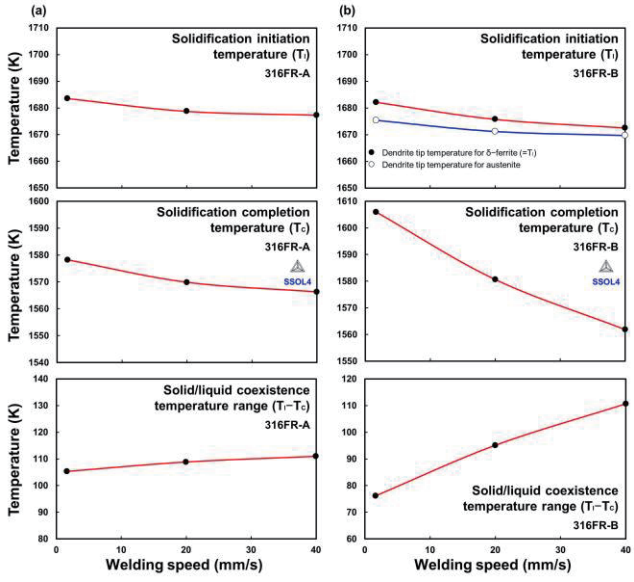

Fig. 6 Calculated solid/liquid coexistence temperature range for (a) 316FR-A and (b) 316FR-B.

4.3 Effect of welding speed on solid/liquid coexistence temperature range

Fig. 6 shows calculation results of T_I, T_C and $T_I - T_C$ as a function of welding speed for 316FR-A and 316FR-B. Although $T_I - T_C$ enlarged for both 316FR-A and 316FR-B, the enlargement range of $T_I - T_C$ for 316FR-B was larger than that of 316FR-A, because of larger decrement of T_C. Namely, the different variation of BTR as a function of welding speed between 316FR-A and 316FR-B was highly correlated with behavior of $T_I - T_C$ for both materials. Also, it could be recognized that $T_I - T_C$ was strongly governed by variation of T_C, which was dominated by the solidification segregation behavior of impurity elements. That is why, the mechanism of the different BTR variation in accordance with welding speed for both 316FR-A and 316FR-B could be explained by the calculation results of $T_I - T_C$, especially focusing on the solidification segregation behavior of impurity elements.

4.4 Variation mechanism of solidification cracking susceptibility in laser welds

It has been commonly regarded that δ-ferrite formation during the welding solidification can play a positive role in the solidification cracking susceptibility, because the ferrite phase possesses the higher solubility of impurity elements (such as S and P) compared with that in austenite phase [4]. The amount of δ-ferrite at solidification completion was calculated based on the model as depicted in Fig. 3 (i.e. area fraction of δ-ferrite phase = area of δ-ferrite phase / total area of the half-quadrangle (ABC)). The ferrite content at solidification completion decreased with an increase in the welding speed from 16 to 10% (for 316FR-A) and 50 to 30% (for 316FR-B), respectively. Although, the ferrite contents decreased with an increase in the welding speed for both materials, the decrement range for 316FR-B (20%) was larger than that for 316FR-A (6%). Namely, the decrement tendency was also different between 316FR-A and 316FR-B. Consequently, through considerations on solidification segregation of impurity elements and the ferrite contents during the welding solidification, the reason of larger increment of the BTR for 316FR-B could be regarded as the larger decrement of the ferrite causing the severe impurities' segregation, thereby more enlarging the solid/liquid coexistence temperature range than as compared with that of 316FR-A.

5. Conclusions

In the present study, solidification cracking susceptibility in laser welds of type 316FR stainless steels was quantitatively evaluated by a transverse-Varestraint test with LBW together with numerical simulations on rapid solidification during LBW. The main conclusions are summarized below.

Solidification cracking susceptibility of two kinds of type 316FR stainless steels with different solidification modes (316FR-A: AF mode solidification, 316FR-B: FA mode solidification) laser welds was quantitatively evaluated by newly developed LBW transverse-Varestraint test. As the welding speed increased from 1.67 (GTAW) to 40.0 (LBW) mm/s, BTR enlarged for both 316FR-A (from 37 to 46 K) and 316FR-B (from 14 to 46 K) welds. The increment range of BTR for 316FR-B was larger than that of 316FR-A. It follows that the variation behavior of solidification cracking susceptibility as a function of welding speed (i.e. application of LBW) was different in accordance with the solidification mode of steel employed. The reason of larger increment of BTR for 316FR-B could be explained by larger decrement of δ-ferrite amount during the welding solidification than that of 316FR-A, affecting further increment of the impurities' segregation (S and P), thereby more enlarging the solid/liquid coexistence temperature range as compared with that of 316FR-A.

Acknowledgements

The present study includes the result of "Core R&D program for commercialization of the fast breeder reactor by utilizing Monju" entrusted to University of Fukui by Ministry of Education, Culture, Sports, Science and Technology of Japan (MEXT).

References

1) E. J. Chun, H. Baba, K. Nishimoto and K. Saida: Effect of sodium on repair-weldability of SUS316FR for fast breeder reactor, Quarterly Journal of Japan Welding Society, 31 (2013), 260-271.
2) K. Saida, Y. Nishijima, H. Ogiwara and K. Nishimoto: Prediction of solidification cracking in laser welds of type 310 stainless steels, Quarterly Journal of Japan Welding Society, 31 (2013), 157-166.
3) E. J. Chun, H. Baba, K. Nishimoto and K. Saida: Development of Varestraint test procedure with laser beam welding and evaluation of solidification cracking susceptibility in austenitic stainless steels (IIW Doc. IX-2480-14, IX-H-793-14), 67th IIW annual assembly, Seoul (2014).
4) S. Kou: Welding metallurgy, A John Wiley & Sons, New York (2003).
5) W. Kurz, B. Giovanola and R. Trivedi: Theory of microstructure development during rapid solidification, Acta. Metall., 34 (1986), 823-930.
6) M. Morishita, H. Ishida and M. Yoshida: Modeling of microsegregation and precipitation of iron metallic compounds in Al-Fe-Si ternary alloy, Journal of Japan Institute of Light Metals, 60, (2010), 157-163.
7) Metals handbook (eds. The Japan Institute of Metals and Materials), Maruzen, Tokyo, (2004).